Dynamic voltage stability analysis in HVDC systems

I. Bedir [a], A.A. Lotfy [b], M.E. AbdelKarim [a] and G.E.M. Aly [a]
[a] *Electrical Power Eng. Dept., Faculty of Eng., Tanta University, Tanta, Egypt*
[b] *Arab Academy for Science and Technology and Maritime Transport, Alexandria, Egypt*

This paper presents a novel analysis of voltage stability at both converter and inverter buses in HVDC systems. The dynamics of DC systems and controllers at different operating conditions are thoroughly considered. The small signal stability model was applied and used to identify the stability margin. The sensitivity of AC and DC system variables is computed at different Short Circuit Ratios (SCR) to illustrate the effect on AC-DC system stability. The results obtained are validated using nonlinear simulation.

تقدم هذه الورقه البحثيه طريقه جديده لتحليل إتزان الجهد فى نظم الجهد الفائق المستمر عند طرفى الموحد و العاكس. وقد تم أخذ التغيرات الديناميكيه لنظم التيار المستمر والمتحكمات فى الإعتبار عند مختلف ظروف التشغيل. وقد تم تطبيق وإستخدام نموذج الإشاره الصغيره للإتزان للتعرف على حدود إتزان النظام. كما تم حساب متغيرات نظم التيار المستمر والمتردد عند مختلف نسب القصر لبيان تأثر إتزان النظام. وقد تم التحقق من النتائج بإستخدام المحاكاه الغير خطيه.

Keywords: HVDC, Volt age stability, SCR

1. Introduction

The available AC systems are being increasingly operated outside their linear domain such that nonlinearities influence system behavior significantly. The Short-Circuit Ratio (SCR) - defined as the ratio of short circuit power at converter bus to the rated DC power - is used to measure the strength of the converter bus. Low SCR values define a weak system where voltage instability is liable to occur. System voltage instability has been widely studied from a nonlinear dynamical system perspective [1]. The power system is thus viewed as a parameter dependent system of Differential-Algebraic Equations (DAE) which defines its underlying qualitative dynamical structure. The system undergoes bifurcations and loss of system stability locally or globally [1, 2]. Several researchers [4, 5, 6] analyzed the problem using static analysis. Nevertheless, voltage instability is a dynamic phenomenon which requires dynamic analysis for accurate prediction [1, 3, 7, 8].

In this paper, the analysis of voltage instability has been carried out considering the dynamics of the DC system using the Eigenvalue analysis and the system response to short circuit ratio variations. The results are compared with that of static analysis. Also the results of small signal stability model are validated using nonlinear simulation.

2. System model

A general rectifier side HVDC system is shown in fig. 1. The HVDC system was considered as an asynchronous interconnection between two or several unconnected AC systems. The ac system was represented by it's thevenin's equivalent at fundamental frequency viewed from the converter bus.

The Voltage Sensitivity (stability) Factor (VSF) is calculated from the relation for a general form HVDC as follows [3]:

$$\Delta U = [VSF]\Delta Q_s \quad . \tag{1}$$

Where $VSF_{(i,j)}$ is the partial derivative of the i^{th} converter bus voltage w.r.t. reactive power supply at the j^{th} converter bus.

2.1. DC system model

The DC system consists of converters, controllers, smoothing reactors and DC lines. The following sets of static equations are used for representing the rectifier and inverter sides respectively [3, 9-11].

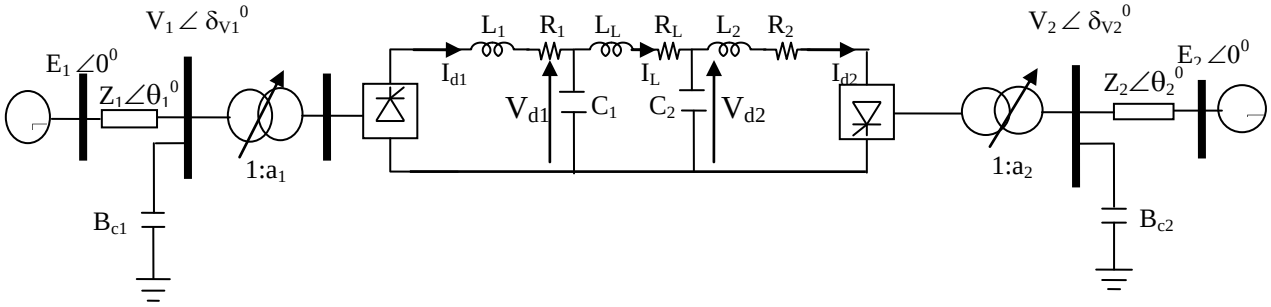

Fig. 1. Complete HVDC system for stability analysis.

$$
\begin{aligned}
&V_{d1} = k_1 a_1 V_1 \cos\alpha_1 - R_{C1} I_{d1} \\
&P_{d1} = B_1 V_{d1} I_{d1} \\
&P_{d1} = B_1 V_{d1} I_{d1} \\
&Q_{d1} = B_1 V_{d1} I_{d1} \tan\phi_1 \\
&\cos\phi_1 = \cos\alpha_1 - (R_{C1} I_{d1})/(k_1 a_1 V_1)\,.
\end{aligned} \tag{2}
$$

$$
\begin{aligned}
&V_{d2} = k_2 a_2 U_2 \cos\beta_2 + R_{C2} I_{d2} \\
&P_{d2} = B_2 V_{d2} I_{d2} \\
&P_{d2} = B_2 V_{d2} I_{d2} \\
&Q_{d2} = B_2 V_{d2} I_{d2} \tan\phi_2 \\
&\cos\phi_2 = \cos\beta + (R_{C2} I_{d2})/(k_2 a_2 V_2) \\
&\cos\gamma = \cos\beta + (2R_{C2} I_{d2})/(k_2 a_2 V_2)\,.
\end{aligned} \tag{3}
$$

2.2. DC network model

The DC network includes converters (rectifier and inverter), smoothing reactors and DC transmission line. The DC transmission line is represented by its π–equivalent. The DC network is shown in the middle of fig. 1. It is represented by the following differential equations:

$$\dot{I}_{d1} = (E_{O1} - R_{C1} I_{d1} - V_{d1})/L_1\,. \tag{4}$$

$$\dot{V}_{d1} = (I_{d1} - I_L)/C_1\,. \tag{5}$$

$$\dot{V}_{d2} = (I_L - I_{d2})/C_2\,. \tag{6}$$

$$\dot{I}_L = (V_{d1} - R_L I_L - V_{d1})/L_L\,. \tag{7}$$

$$\dot{I}_{d2} = (V_{d2} - R_{C2} I_{d2} - E_{O2})/L_2\,. \tag{8}$$

Where $E_{O1} = k_1 a_1 U_1 \cos\alpha$

and $E_{O2} = k_I a_I U_I \cos\beta_I$

L_R and L_I are the sum of smoothing reactor and converter transformer inductances at the rectifier and inverter side respectively.

2.3. DC system controllers

The DC system controller consists of either a current, power, voltage or constant delay angle controller at rectifier side. The inverter controller consists of either a current, power, voltage, constant extinction angle or constant advance angle controller. The differential equations of a PI current controller at rectifier side can be written as follows [1, 3]:

$$\dot{x}_{cR} = k_{IR}(I_{d1} - I_{o1})\,. \tag{9}$$

$$\alpha_R = x_{cR} + k_{PR}(I_{d1} - I_{o1})\,. \tag{10}$$

2.4. AC system model

The active and reactive power flow through AC lines in both rectifier and inverter can be written as follows:

$$
\begin{aligned}
&P_{ac1} = V_1^2 Y_1 \cos\theta_1 + V_1 E_1 Y_{1E} \cos(\theta_{1E} - \delta_{v1}) \\
&P_{ac2} = V_2^2 Y_2 \cos\theta_2 + V_2 E_2 Y_{2E} \cos(\theta_{2E} - \delta_{v2}) \\
&Q_{ac1} = -V_1^2 Y_1 \sin\theta_1 - V_1 E_1 Y_{1E} \sin(\theta_{1E} - \delta v_1) \\
&Q_{ac2} = -V_2^2 Y_2 \sin\theta_2 - V_2 E_2 Y_{2E} \sin(\theta_{2E} - \delta_{v2})\,.
\end{aligned} \tag{11}
$$

Where

$\overline{Y}_1 = 1/\overline{Z}_1 + jB_{C1} = Y_1\angle\theta_1$ and
$\overline{Y}_2 = 1/\overline{Z}_2 + jB_{C2} = Y_2\angle\theta_2$
$\overline{Y}_{1E} = 1/\overline{Z}_1 = Y_{1E}\angle\theta_{1E}$, and
$\overline{Y}_{IE} = 1/\overline{Z}_I = Y_{IE}\angle\theta_{IE}$
$\overline{Z}_1 = R_1 + jX_1 = Z_1\angle\theta_1$ and
$\overline{Z}_2 = R_2 + jX_2 = Z_2\angle\theta_2$

2.5. Small signal stability model

The system differential equations can be linearized to obtain the state space model:

$$\dot{x}_{DC} = A\,x_{DC} + B\,u_{DC}\ . \tag{12}$$

The system algebraic equations can be written as follows:

$$P_{acR} + P_{dR} = 0$$
$$P_{acI} - P_{dI} = 0\,. \tag{13}$$

$$Q_{acR} + Q_{dR} = 0$$
$$Q_{acI} + Q_{dI} = 0\,. \tag{14}$$

By linearizing eqs. (13 and 14), the state space form of algebraic equations is obtained:

$$0 = Cx_{DC} + Du_{DC}\,. \tag{15}$$

Where "*C*", and "*D*" are the Jacobian submatrices.

Assuming that *D* remains nonsingular along system trajectories as the system parameters vary, then eqs. (12 and 15) are reduced to:

$$\dot{x}_{DC} = A'\,x_{DC}\,. \tag{16}$$

Where $A' = A - BD^{-1}C$.

Eq. (16) represents the small signal stability model of DAE suitable for HVDC system. Voltage stability analysis is carried out by computing Eigenvalues of system state matrix A'.

3. Solution methodology

This paper proposes an exact analysis that incorporates load flow using Newton-Raphson method at each operating condition defined by an SCR value. The integration of power flow in the analysis is needed to cope with the changes in the AC system leading to a change in the short circuit ratio. Otherwise, the results will not be justified. The methodology is illustrated in fig. 2.

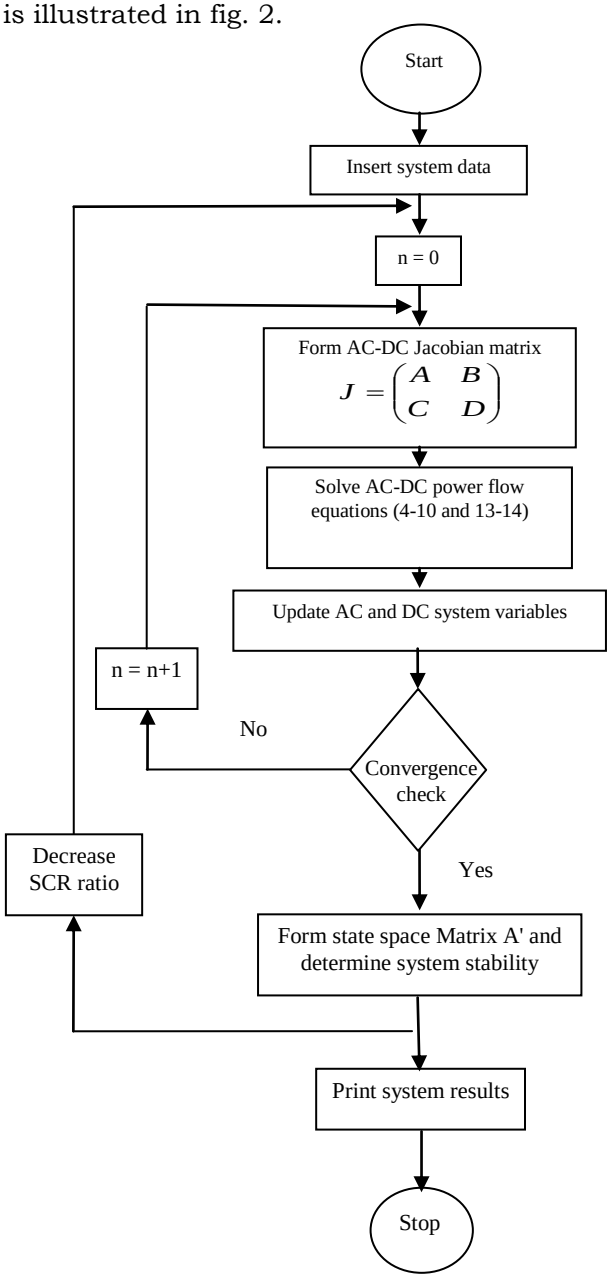

Fig. 2. Solution methodology flow-chart.

4. Case study

The data of the HVDC system used to implement the proposed technique is given in table 1.

Fig. 3-a shows the change of line voltages at both rectifier and inverter buses as a function of SCR_{Inv} (reduced from an initial value of 3.0). The rectifier is on CC and the inverter is on Cγ control. The line voltage at inverter side is found to be more sensitive to the decrease of SCR compared with that of the rectifier side. Hopf bifurcation occurs when SCR_{Inv} is decreased to 1.97122.

Fig. 3-b shows the phase shift at both rectifier and inverter bus as a function of SCR_{Inv}. The increase of phase shift at inverter bus with SCR decrease is greater than that at the rectifier bus. The outcomes of figs. 3-a, 3-b are consistent and furthermore demonstrate the deterioration of stability at low SCR values.

Fig. 3-c shows the change of DC line voltages at both rectifier and inverter as a function of SCR_{Inv}. DC voltages decrease subsequently as a result of the decrease of AC line voltage.

Fig. 3-d demonstrates the change of VSF at inverter as a function of SCR_{Inv}. The VSF_{Inv} is increased with the decreasing of SCR_{Inv} but it remains positive which means the system is still stable until SCR_{Inv} equals 1.392176 from static analysis perspective. Nevertheless, dynamic analysis shows that instability is reached at 1.97122 (Hopf bifurcation).

Fig. 3-e demonstrates a sensitivity analysis without power flow of VSF_{Inv} as a function of SCR_{Inv}. Accordingly, the system's loss of stability will not occur until SCR_{Inv} is decreased to 0.6268 from static analysis perspective and 1.604364 (Hopf bifurcation) from dynamic analysis perspective. Both optimistic outcomes demonstrate the importance of incorporating load flow for accurate stability analysis.

Fig. 4-a shows the change of line voltages at both rectifier and inverter buses as a function of SCR_{Rect}. The rectifier is on CDA and the inverter is on CC control. The line voltage at rectifier side is found to be more sensitive to the decrease of SCR compared with that of the inverter side. Saddle node

Table 1
AC and DC lines data (p.u.)

AC line data (p.u.)					
Terminal	E	R_C	L	X	B_C
Rectifier	1.1	0.115	0.0052	0.2857	0.4
Inverter	1.1	0.115	0.0052	0.3333	0.6

DC line data (p.u.)			
R_L (p.u.)	L_L	C_1	C_2
0.04462	0.0008235	0.000272	0.000272

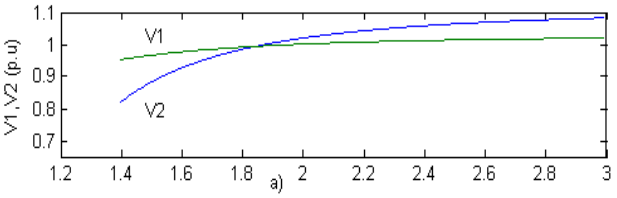

a) V_1 and V_2 versus SCR_{Inv}.

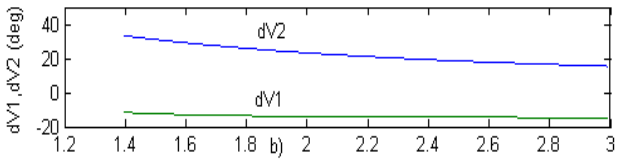

b) d_{v1} and d_{v2} versus SCR_{Inv}.

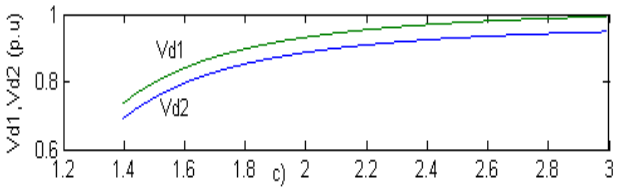

c) V_{d1} and V_{d2} versus SCR_{Inv}.

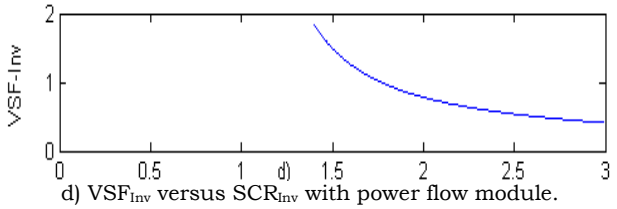

d) VSF_{Inv} versus SCR_{Inv} with power flow module.

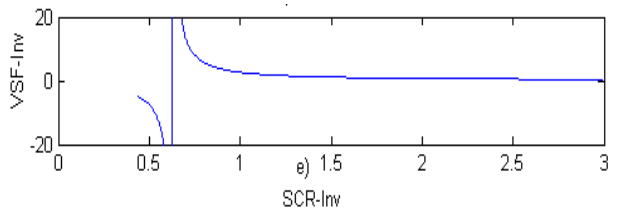

e) VSF_{Inv} versus SCR_{Inv} with power flow module deactivated after initialization.

Fig. 3. System variables for CC/Cγ control mode.

bifurcation occurs when SCR_{Inv} is decreased to 1.942879.

Fig. 4-b shows the phase shift at both rectifier and inverter bus as a function of SCR_{Rect}. The increase of phase shift at rectifier bus with SCR decrease is greater than that at the inverter bus. The outcomes of figs. (4a, 4.b) are consistent and furthermore demonstrate the deterioration of stability at low SCR values.

Fig. 4-c shows the change of DC line voltages at both rectifier and inverter as a function of SCR_{Rect}. DC voltages decrease subsequently as a result of the decrease of AC line voltage.

Fig. 4-d demonstrates the change of VSF_{Rect} at rectifier as a function of SCR_{Rect}. The $VSF_{Rect.}$ is increased with the decreasing of SCR_{Rect} but it remains positive which means the system is still stable until SCR_{Rect} equals 1.247349 from static analysis perspective. Nevertheless, dynamic analysis shows that instability is reached at 1.942879 (Saddle node bifurcation).

Fig. 4-e demonstrates a sensitivity analysis without power flow of $VSF_{Rect.}$ as a function of $SCR_{Rect.}$. Accordingly, the system's loss of stability will not occur until $SCR_{Rect.}$ is decreased to 0.27385 from static analysis perspective and 1.183852 (Saddle node bifurcation) from dynamic analysis perspective. Both optimistic outcomes demonstrate the importance of incorporating load flow for accurate stability analysis.

Fig. 5 corresponds to a stable case (SCR_{Inv} = 3.0), the rectifier is on CC control while the inverter is on Cβ control. Fig. 5-a shows the time response of DC line current at both rectifier and inverter. A small change will occur in inverter current due to CC in inverter side while a large change occurs in rectifier side current which reaches steady state after 0.2 sec.

Fig 5-b shows the phase plane of DC line voltage against DC line current at the inverter side. The figure illustrates that both DC voltages reach a stable node point.

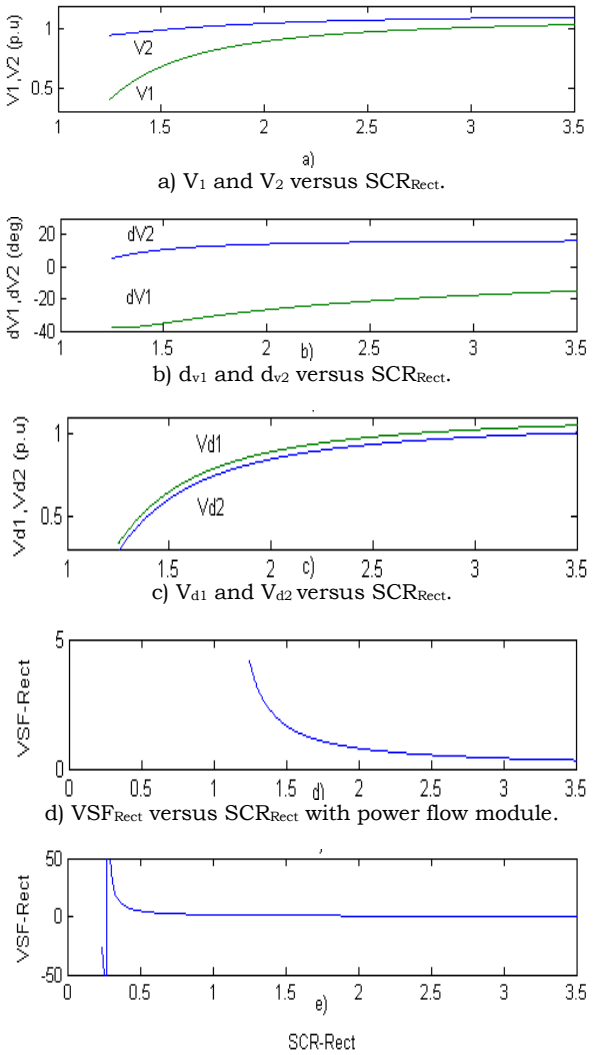

a) V_1 and V_2 versus SCR_{Rect}.

b) d_{v1} and d_{v2} versus SCR_{Rect}.

c) V_{d1} and V_{d2} versus SCR_{Rect}.

d) VSF_{Rect} versus SCR_{Rect} with power flow module.

e) VSF_{Rect} versus SCR_{Rect} with power flow module deactivated after initialization.

Fig. 4. System variables for CDA/CC mode.

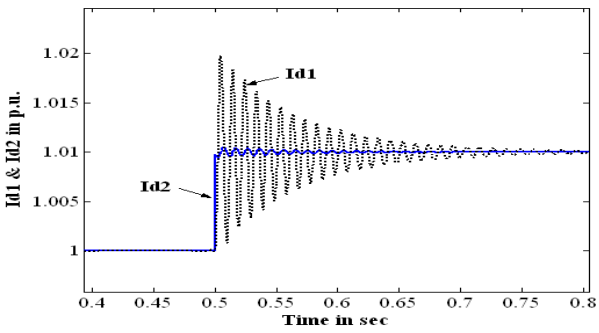

Fig. 5-a. Response of dc currents due to step change in inverter current order from 1.0 to 1.01 p.u. at t = 0.5 sec. (SCR = 3.0).

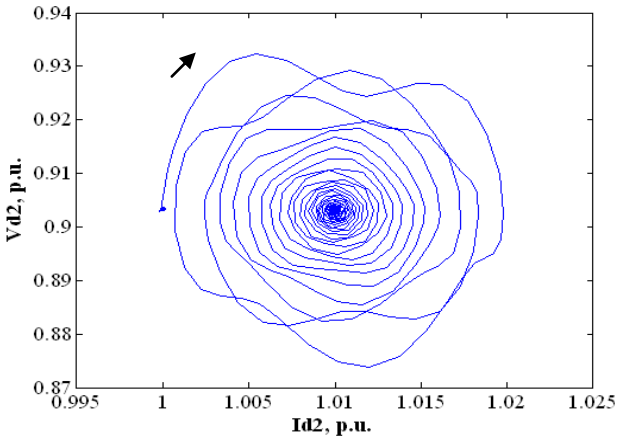

Fig. 5-b. phase plane of V_{d2} and I_d2 due to step change in inverter current order from 1.0 to 1.01 p.u. at t = 0.5 sec.

Fig. 6 corresponds to an unstable case; $SCR_{Inv.}$ = 2.529724 (Hopf Bifurcation). The rectifier is on CC control while the inverter is on Cβ control. Fig. 6-a shows the time response of DC line current at both rectifier and inverter. A small change occurs in inverter current due to CC controller in inverter side while a large change occurs in rectifier current which oscillates around an unstable node. Fig. 6-b shows the phase plane of DC line voltage against DC line current which illustrates that they oscillate around unstable node point. Fig. 6-c shows the phase plane of AC line voltage against DC line voltage which illustrates that they oscillate around unstable node point.

Tables 2 and 3 demonstrate the dynamic and static analysis instability boundaries of different control modes of HVDC system with and without power flow implementation.

5. Stability improvement

The system stability can be improved through control mode selection and / or reactive power injection at converter bus.

Fig. 7 shows the effect of inserting 0.1 p.u. reactive power at rectifier bus for the case of CDA/CC control. The system was found to maintain its stability until SCR_{Inv} is decreased to 1.796300 instead of 1.942879.

Table 2
Critical SCR (Incorporating power flow)

Control mode	Dynamic analysis	Static analysis
CDA/CC	1.942879 (SN)	(SCR>= 1.247349)
CDA/CP	2.558700 (SN)	2.5587
CC/Cγ	1.971220 (HP)	(SCR>= 1.392176)
CC/Cβ	2.529724 (HP)	Stable until power flow failed at 0.965904
CDV/ CC	1.942879 (SN)	Stable until power flow failed at 1.247349
CP/Cβ	2.443196 (HP)	Stable until power flow failed at 1.461300
CDV/CP	2.613013 (SN)	Stable until power flow failed at 2.559500

Table 3
Critical SCR (without power flow)

Control mode	Dynamic analysis	Static analysis
CDA/CC	1.183852 (SN)	0.273850
CDA/CP	1.371742 (SN)	1.371742
CC/Cγ	1.604364 (HP)	0.626800
CC/Cβ	2.292001 (HP)	0.336780
CDV/ CC	1.190902 (SN)	Stable for all SCR
CP/Cβ	2.201189 (HP)	0.826240
CDV/CP	1.190902 (SN)	Stable for all SCR

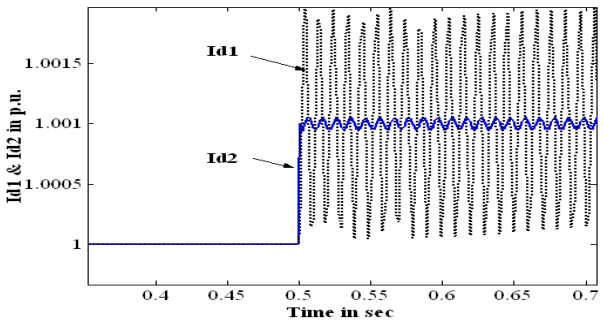

Fig. 6-a. Time response of I_{d1} and I_{d2} due to step change in inverter current order from 1.0 to 1.001 p.u. at t =1.0 sec at a SCR of 2.529.

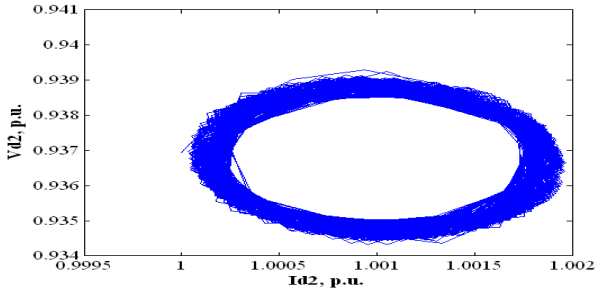

Fig. 6-b. phase plane of V_{d2} and I_{d2} due to step change in inverter current order from 1.0 to 1.01 p.u. at t =1.0 sec at a SCR of 2.529.

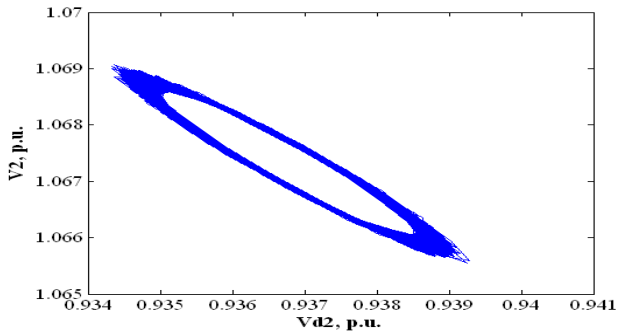

Fig. 6-c. phase plane of V_2 and I_{d2} due to step change in inverter current order from 1.0 to 1.001 p.u. at t =1.0 sec at a SCR of 2.529.

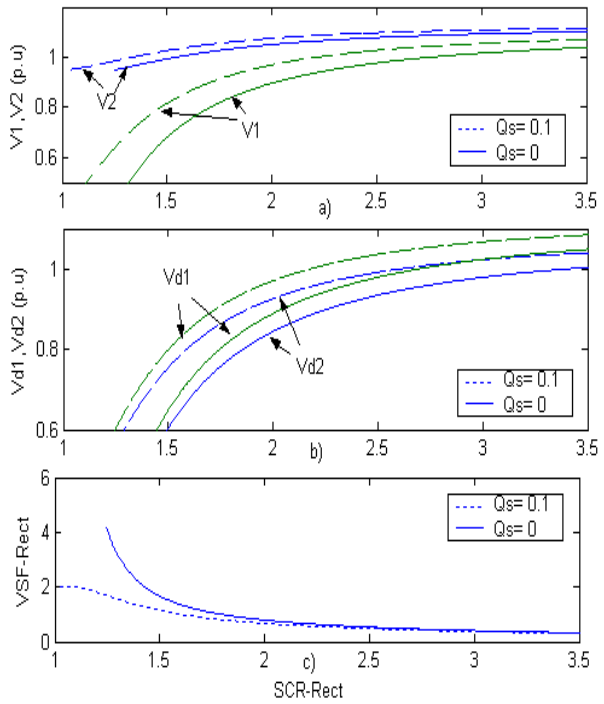

Fig. 7. Effect of reactive power injection.

6. Conclusions

A novel voltage stability analysis for HVDC systems is proposed. The procedure considers both of the dynamics of DC systems and controllers at different operating conditions.

The incorporation of a load flow module resulted in truly defined stability boundaries. This in turn facilitates control corrective actions in case of system topology changes during faults and / or switching operations.

The procedure was applied with different control modes at both rectifier and inverter sides. The results revealed the importance of the technique to HVDC system planners and operators.

Symbols

P_{d1}, Q_{d1}, P_{d2} and Q_{d2}	are the rectifier and inverter DC active and reactive power respectively,
P_{ac1}, Q_{ac1}, P_{ac2}, and Q_{ac2}	are the active and reactive power in AC lines in both rectifier and inverter respectively,
Q_S	is the reactive power injected at converter bus,
α, β and γ	are the rectifier delay angle and inverter advance and extinction angle respectively,
$\cos\phi_1$ and $\cos\phi_2$	are the rectifier and inverter power factors,
k_1 and k_2	are the rectifier and inverter constant,
CC, $C\gamma$, $C\beta$, CDA, CP, CD and V	are the constant current, aconstant gamma, constant beta, constant delay angle, constant power and constant DC voltage controllers respectively,
x_{DC} and u_{DC}	are the represent the mismatch of system state variables and DC system inputs,
R_L and L_L	are the DC line resistance and reactance,
d_{v1} and d_{v2}	are the rectifier and inverter bus phase angles,
L and X	are the commutation inductance and AC transmission line reactance respectively,
k_{IR} and k_{PR}	are the integral and proportional current controller gain respectively,
x_{cR}	is the output of integral controller branch, and
SN and HP	is the saddle node and Hopf bifurcations.

Appendix

$$AC\text{-}DC\ Jacobian = \begin{bmatrix} A & B \\ C & D \end{bmatrix}$$

where,

$$A=\begin{bmatrix}0 & A_{12} & 0 & 0 & 0 & 0\\ A_{21} & A_{22} & A_{23} & 0 & 0 & 0\\ 0 & 0 & A_{33} & 0 & A_{35} & 0\\ 0 & A_{42} & 0 & 0 & 0 & A_{46}\\ 0 & 0 & A_{53} & 0 & 0 & A_{56}\\ 0 & 0 & 0 & A_{64} & A_{65} & A_{66}\end{bmatrix},$$

$$B=\begin{bmatrix}0 & 0 & 0 & 0\\ B_{21} & 0 & 0 & 0\\ 0 & 0 & B_{33} & 0\\ 0 & 0 & 0 & 0\\ 0 & 0 & 0 & 0\\ 0 & 0 & 0 & 0\end{bmatrix}$$

$$C=\begin{bmatrix}0 & C_{12} & 0 & C_{14} & 0 & 0\\ 0 & 0 & C_{23} & 0 & C_{25} & 0\\ C_{31} & C_{32} & 0 & C_{34} & 0 & 0\\ 0 & 0 & C_{53} & 0 & C_{55} & 0\end{bmatrix},$$

$$D=\begin{bmatrix}D_{11} & 0 & D_{31} & 0\\ 0 & D_{22} & 0 & D_{24}\\ D_{31} & 0 & D_{33} & 0\\ 0 & D_{42} & 0 & D_{44}\end{bmatrix}$$

$$A_{12}=k_{i1}$$

$$A_{21}=-k_1 * a_1 * V_1 * \sin(x_{c1}+k_{p1}*(i_{d1}-i_{ref\,1}))/L_1$$

$$A_{22}=(-k_1 * a_1 * V_1 * \sin(x_{c1}+k_{p1}*(i_{d1}-i_{ref\,1}))*k_{p1}-R_{c1})/L_1$$

$$A_{23}=-1/L_1$$

$$A_{32}=-R_{c2}/L_2 \backslash$$

$$A_{35}=1/L_2$$

$$A_{42}=1/C_1$$

$$A_{46}=-1/C_1$$

$$A_{53}=-1/C_1$$

$$A_{56}=1/C_1$$

$$A_{64}=1/L_L$$

$$A_{65}=-1/L_L$$

$$A_{65}=-R_L/L_L$$

$$B_{21}=k_1 * a_1 * \cos(x_{c1}+k_{p1}*(i_{d1}-i_{ref\,1}))/L_1$$

$$B_{33}=-k_2 * a_2 * \cos(\beta)/L_2$$

$$C_{12}=V_{d1}$$

$$C_{14}=i_{d1}$$

$$C_{23}=-V_{d2}$$

$$C_{25}=-i_{d2}$$

$$C_{31}=v_{d1}i_{d1}/[\sqrt{(1-(\cos(x_{c1}+k_{p1}(i_{d1}-i_{ref\,1}))-R_{c1}i_{d1}/(k_1a_1v_1))^2}\,)\times\sin(x_{c1}+k_{p1}(i_{d1}-i_{ref\,1}))+v_{d1}i_{d1}\times\sqrt{(1-(\cos(x_{c1}+k_{p1}(i_{d1}-i_{ref\,1}))-Rc1/k1/a1*id1/v1)^2}\,]/[(\cos(x_{c1}+k_{p1}(i_{d1}-i_{ref\,1}))-R_{c1}i_{d1}/(k_1a_1v_1))^2\times\sin(x_{c1}+k_{p1}*(i_{d1}-i_{ref\,1}))]$$

$$C'_{32}=\frac{v_{d1}\sqrt{[1-(\cos(x_{c1}+k_{p1}(i_{d1}-i_{ref\,1}))-R_{c1}i_{d1}/(k_1a_1V_1)]^2}}{\sqrt{(\cos(x_{c1}+k_{p1}(i_{d1}-i_{ref\,1}))-R_{c1}i_{d1}/(k_1a_1V_1))-v_{d1}i_{d1}/(1-(\cos(x_c1+k_{p1}(i_{d1}-i_{ref\,1}))-R_{c1}i_{d1}/(k_1a_1V_1))^2}}$$

$$C''_{32}=\frac{\sqrt{[-\sin(x_{c1}+k_{p1}(i_{d1}-i_{ref\,1}))k_{p1}-R_{c1}/(k_1a_1V_1))-v_{d1}i_{d1}(1-(\cos(x_{c1}+k_{p1}(i_{d1}-i_{ref\,1}))-R_{c1}i_{d1}/(k_1a_1v_1))]}}{[\cos(x_{c1}+k_{p1}(i_{d1}-i_{ref\,1}))-R_{c1}/(k_1a_1V_1))^2(-\sin(x_{c1}+k_{p1}(i_{d1}-i_{ref\,1}))k_{p1}-R_{c1}/(k_1a_1V_1)]}$$

$$C_{25}=C'_{32}\,C''_{32}$$

$$C_{34}=\frac{id1\sqrt{1-(\cos(x_{c1}+k_{p1}(i_{d1}-i_{ref\,1}))-R_{c1}i_{d1}/(k_1a_1V_1))^2}}{\cos(x_{c1}+k_{p1}*(i_{d1}-i_{ref\,1}))-R_{c1}i_{d1}/(k_1a_1V_1)}$$

$$C_{43}=v_{d2}(\sqrt{1-(\cos(\beta)+R_{c2}i_{d2}/(k_2a_2V_2))^2}\,)/\sqrt{[\cos(\beta)+R_{c2}i_{d2}/(k_2a_2V_2))/(1-(\cos(\beta)+R_{c2}i_{d2}/(k2a2v2))^2}\,]\times R_{c2}i_{d2}/(k_2a_2V_2)-i_{d2}v_{d2}(1-(\cos(\beta)+R_{c2}i_{d2}/(k_2a_2V_2))^2R_{c2}/(k_2a_2V_2)$$

$$C_{45}=id2[1-\sqrt{(\cos(\beta)+R_{c2}i_{d2}/(k_2a_2V_2))^2}\,)/(\cos(\beta)+R_{c2}i_{d2}/(k_2a_2V_2)]$$

$$D_{11} = 2V_1 y_{c1}\cos(\theta_{c1}) + E_1 y_{ce1}\cos(th_{ce1} - d_{v1})$$

$$D_{13} = V_1 E_1 y_{ce1}\sin(\theta_{ce1} - d_{v1}))$$

$$D_{22} = 2V_2 y_{c2}\cos(\theta_{c2}) + E_2 y_{ce2}\cos(th_{ce2} - d_{v2})$$

$$D_{24} = -V_2 E_2 y_{ce2}\sin(\theta_{ce2} - d_{v2}))$$

$$D_{31} = -2V_1 y_{c1}\sin(\theta_{c1}) - E_1 y_{ce1}\sin(\theta_{ce1} - d_{v1}) - v_{d1} i^2{}_{d1} / \sqrt{(1 - (\cos(x_{c1} + k_{p1} * (id1 - iref1)) - R_{c1} i_{d1} / (k_1 a_1 V_1))^2)} \times$$

$$\sqrt{(1 - (\cos(xc1 + k_{p1} * (i_{d1} - i_{ref\,1})) - R_{c1} i_{d1} / (k_1 a_1 V_1))^2)} \times (\cos(x_{c1} + k_{p1}(i_{d1} - i_{ref\,1})) - R_{c1} i_{d1} / (k_1 a_1 V_1^2)$$

$$D_{33} = V_1 E_1 y_{ce1}\cos(\theta_{ce1} - d_{v1}))$$

$$D_{42} = -2V_2 y_{c2}\sin(\theta_{c2}) + E_2 y_{ce2}\sin(-\theta_{ce2} + d_{v2}) + i^2{}_{d2} v_{d2} / \sqrt{(1 - (\cos(\theta_2) + R_{c2} i_{d2} / (k_2 a_2 v_2))^2)} \times$$

$$R_{c2} / (k_2 a_2 v^2{}_2)) + i^2{}_{d2} v_{d2} \sqrt{(1 - (\cos(\theta_2) + R_{c2} i_{d2} / ((k_2 a_2 v_2))^2} / (\cos(\theta_2) + R_{c2} i_{d2} / (k_2 a_2 v_2))^2 R_{c2} / (k_2 a_2 v^2{}_2)$$

$$D_{44} = V_2 E_2 y_{ce2}\cos(-\theta_{ce2} + d_{v2}))$$

References

[1] Denis Lee Hau Aik and G. Anderson, "Nonlinear Dynamics in HVDC Systems", IEEE Transactions on Power Delivery, Vol. 14 (4), p. 1417 (1999).

[2] N. Mithulananthan Claaudio A. Ganizares John Reeve, "Indices to Detect Hopf Bifurcations in Power Systems", NAPS-2000, p. 1 (2000).

[3] K.R. Padiyar and S.S. Rao, "Dynamic Analysis of Voltage in AC-DC Systems", Elsevier Science Ltd. Electrical Power and Energy Systems, Vol. 18 (1), p. 11 (1996).

[4] B. Franken and G. Anderson, "Analysis of HVDC Converters Connected to weak AC Systems", IEEE Trans. on Power Systems. Vol. 5 (1), p. 235 (1990).

[5] D. Lee, H. Aik and G. Anderson, "Voltage Stability Analysis Multi-Infeed HVDC Systems", IEEE Transactions on Power Delivery. Vol. 12 (3), p. 1309 (1997).

[6] D. Jovcic, N. Pahalawaththa and M. Zavahir, "Small Signal Analysis of HVDC-HVAC Interconn ections", IEEE Trans. on Power Delivery. Vol. 14 (2), p. 525 (1999).

[7] L.A.S. Pilotto, M. Szechtman and A.E. Hammad "Transient AC Voltage Related Phenomena for HVDC Schemes Connected to Weak AC Systems", IEEE Transactions on Power Delivery. Vol. 7 (3), p. 1396 (1992).

[8] X. Yang and C. Chen, "HVDC Dynamic Modeling of Small Signal analysis", IEE Proc. Gen., Trans. and Dist., Vol. 151 (6), p. 740 (2004).

[9] O.B. Nayak et al., "Control Sensitivity Indices for Stability Analysis of HVDC Systems'', IEEE Trans. on Power Delivery, Vol. 10 (4), p. 2054 (1995).

[10] Y.K. Fan et al., "Multiple Power Flow Solutions of Small Integrated AC/DC Power System'', IEEE Int. Symposium on Circuits and Systems, Vol. 2, Switzerland, p. 224 (2000).

[11] P. Kundur, "Power System Stability and Control", McGraw-Hill, Inc., (1994).

Received August 12, 2006
Accepted December 26, 2006